

1 **Role of self-propulsion of marine larvae on their probability**
2 **of contact with a protruding collector located in a sea current**

3 Gregory Zilman^{1*}, Julia Novak¹, Alex Liberson¹, Shimrit Perkol-Finkel¹, Yehuda
4 Benayahu²

5 1. School of Mechanical Engineering, Tel-Aviv University, 69978, Israel, 2. School of
6 Life Science, Tel- Aviv University, 69978, Israel.

7

8 Settlement of marine larvae on a substrate is a fundamental problem of marine life.
9 The probability of settlement is one of the quantitative characteristic of the settlement
10 process. The probability of larval contact with a substrate is the upper bound of the
11 probability of settlement. This work addresses the problem of contact probability and
12 contact rate of marine invertebrate larvae with an isolated protruding collector located
13 in an unbounded sea current. There are two common approaches to the problem of
14 contact probability. In one, a collector induces certain cues, which help a larvae find
15 the collector. In such a case, the larva moves towards the collector deliberately, using
16 its navigation and propulsion devices. In the second approach, a larva moves towards
17 a collector as a passive small particle. In this case, the cause of contact of a larva with a
18 collector is a mechanical collision of a small moving body with a large obstacle. We
19 considered a larva which does not know the location of the collector, which does not
20 use its navigation device yet uses its self-propulsion. We mimiced a larva by a tiny
21 self-propelled underwater vehicle, moving in shear flow of a large obstacle. We
22 illustrated our approach by studying contact of a larva of the Bryozoan *Bugula neritina*
23 with a cylindrical collector. We observed the behavior of this larva in a laboratory
24 flume, and according to the observations formulated a mathematical model of larval
25 motion in shear flow. The trajectories of a large number of larvae, starting their motion
26 far from a collector with random initial conditions are calculated numerically, and the
27 probability of their contact with a collector is estimated. The results of Monte-Carlo
28 simulations illustrate that larval self-propulsion may increase the probability of their
29 contact with a collector by orders of magnitude compared to passive particles.

30 **KEYWORDS:** larvae; *Bugula neritina*; settlement; protruding collector; contact
31 probability; collision efficiency; self-propulsion; hydrodynamics; mathematical model

32

33

34

35 **Introduction**

36

37 A number, which is called the *probability of settlement*, is often used in the
38 biological literature to characterize the proportion of larvae that have settled on a
39 specific substratum to the total number of larvae that could possibly settle on this
40 substratum under the same biological and physical conditions [1].

41 It is common to distinguish between larval collectors of infinite extent
42 (e.g., plane substrates) and finite size collectors. Our work examines settlement of
43 larvae on a protruding isolated collector, a problem that, to date, has received
44 much less attention despite its importance.

45 The probability of settlement is a product of the probability of contact with
46 and the probability of attachment to a collector. Contact precedes attachment.
47 Hence, the probability of contact represents the upper bound of the settlement
48 probability. This number is also of a great interest in marine biology, especially if
49 settlement follows the first contact event [10].

50 The geometry of natural finite size collectors is difficult to describe
51 precisely. For achieving a better understanding of the complex settlement
52 phenomenon it is also common to study settlement of larvae on/in bodies of well-
53 defined geometry, such as tubes [2-3], plates [1], [4-6] or cylinders [7-9]. Our
54 work examines contact of larvae with a long vertical cylinder located in an
55 unbounded sea current.

56 Given that far from a collector the velocity of the sea current is typically
57 much higher than the swimming velocity of a larva, the larva's motion toward a
58 collector is generally regarded as transport of a passive particle. If a larva always
59 behaves as a passive particle, then its contact with a collector can be studied
60 within the framework of the theory of aerosols and hydrosols, in which the
61 probability of contact of a large number of identical passive particles with a
62 collector is termed the collector's *collision efficiency* [11]. A definition of the
63 collision efficiency of passive particles which is adopted from the theory of
64 aerosols and hydrosols [11]. For an unbounded flow it is defined as the ratio of the
65 number of particles n_c striking the collector to the number of particles N that
66 would have passed through it if they moved along ballistic trajectories (i.e., along
67 straight lines) [11]:

$$68 \quad E = \lim_{N \rightarrow \infty} \frac{n_c}{N}. \quad (1)$$

69 An important characteristic of a collector of particles is the rate of contacts of
70 particles with the collector, i.e., the number of larvae that contact a characteristic
71 area of a collector in a unit of time t :

$$72 \quad \frac{dE}{dt} = CEU_{\infty} S, \quad (2)$$

73 where the concentration number C is the number of larvae in a unit volume of the
74 bulk water. The collision efficiency of a collector and the contact rate of collision
75 are strongly related characteristics: (2) follows from (1). However, for biological
76 applications the rate of contacts may be a more convenient characteristics than the
77 collision efficiency of a collector which may be very low because tiny particles in
78 the velocity field of a large collector move approximately along stream lines
79 which do not cross the surface of the collector.

80 Due to the very low collision efficiency of collectors of tiny passive particles
81 [11-14], some researchers consider water flow as a "*hydrodynamic impediment*"
82 to larval settlement [15] (see also the corresponding argumentation in Fig. 1).
83 Larva may increase its odds to make contact with a collector by increasing the
84 radius of contact Δ , e.g., by increasing the volume of its body or by protruding
85 long mucous threads [10], [15]. A larva may also sense a collector and navigate
86 toward it via attraction by various cues, including diluted chemical material or
87 biofilms [16-19]. In turn, it can be argued that many larvae of marine
88 invertebrates (e.g. the bryozoan *Bugula neritina*) are not capable of significantly
89 increasing their contact radius, or may settle on clean surfaces [2-3], which
90 seemingly excludes the role of chemical cues during the process of selecting a
91 substrate for settlement.

92 In this work, we present a mathematical model of larval contact with a collector
93 that differs from a model of passive contact by one factor. As in the concept of
94 passive contact, we assume that the collector does not induce any cues, a larva
95 does not know where the collector is located, and does not increase its contact
96 radius. However, a larva is self-propelled. Although the words "larva" and
97 "particle" are not synonyms, we use them interchangeably. We consider a larva
98 as a self-propelled particle. In our formulation, the larva moves as an underwater
99 vehicle equipped with a propulsor but whose navigation device is not functioning.
100 If such a vehicle meets a large obstacle located in unbounded sea the sea current,
101 e.g. in a large vortex, is the collision with the obstacle unavoidable or avoidable?
102 If the same vehicle repeats its motion many times but with different initial
103 conditions, what is the probability of collision? Similar questions are frequently
104 asked in the theory of marine vessel control [20-21]; whereas similar aspects of
105 the motion of a self-propelled marine larva in a large vortex were studied in [22-
106 24]. Despite a huge difference in the scales of a marine vehicle and a larva, the
107 vehicle and the larva moving in a fluid obey certain general laws of mechanics
108 and hydrodynamics that have much in common for such different objects.

109 The structure of the paper is as follows. We first describe trajectories of *B.*
110 *neritina* larvae measured in a laboratory flow tank. The analysis of the trajectories
111 allowed us to develop a simple description of a larva's typical helical motion and
112 estimate the relevant parameters of the helix, which are included in the
113 mathematical model of motion of a larva. For computing the velocity field in the
114 proximity of a collector, we used a commercial computational fluid dynamic
115 (CFD) package, ANSYS-FLUENT 13.0 (hereafter AF13) [25], and the methods
116 of classical boundary layer theory [26]. The probability of contact of larvae with a
117 collector was calculated by using the Monte-Carlo method [27], i.e., by simulating
118 a large number of larvae trajectories with random initial conditions. Next, we
119 show that self-propulsion may greatly increase the odds of a larva to make contact
120 even if the location of the collector is unknown.

121 Results

122 Due to a huge variety of larval forms, a mathematical model of a larva's
123 motion cannot be rather general. In each particular case, the parameters that may
124 be necessary for mathematical modeling of larval motion can only be found
125 experimentally. As a basis of our mathematical we chosed the bryozoan larva of
126 *B. neritina*. If a larva can be considered as a mechanical object, we expect that the
127 essential features of a mathematical model of motion of *B. neritina* may have
128 much in common with mathematical models of the motion of other self-propelled
129 larva.

130

131

132 Parameters of a larva and of its typical trajectory

133 A photograph of the body of a *B. neritina* larva, as seen under an electron
134 microscope, is shown in Fig. 2. The shape of the larvae is similar to a prolate
135 spheroid with a length to maximal width ratio of 1.1 approximately. Such spheroid
136 can be approximated by a sphere of the same volume i.e., an equivalent sphere with
137 a radius of $d_p = 200 - 350 \mu\text{m}$ [28-29]. Once the approximate volume of an
138 equivalent sphere is known, the difference of the mean density of the body of a larva
139 ρ_p and the water density ρ_f can be estimated using the sinking velocity of an
140 immobilized larva, of the order of $V_t \approx 1 \text{mm/s}$ [30]. Although the drag of a smooth
141 sphere and of a ciliated larva are not the same [31] using Stokes' formula provides a
142 correct order of magnitude of the ratio $\rho_p / \rho_f \sim 1.1$.

143 Trajectories of larvae in a laboratory flume are shown in Fig. 3. Enlarged
144 sections of the trajectories are separately plotted in Fig. 4. In Figures 3-4 larvae
145 typically moved along a path, which can approximately be described by a helix (Fig.
146 5).

147 A helix is drawn by the end of a line of length a , which rotates about an
148 axis $o\xi$ with constant angular frequency γ and translates simultaneously along
149 this axis with constant velocity V_s . The angular frequency γ and the temporal
150 period of a helix T are related as $\gamma = 2\pi/T$. When a certain point of a helix
151 makes a full turn, it translates along the axis of the helix at distance P , which is
152 called the pitch of the helix. The trajectory of a point of a helix can be described
153 in a Cartesian coordinate system $o\xi\eta\zeta$ with unit vectors of the axes $(\mathbf{i}_\xi, \mathbf{i}_\eta, \mathbf{i}_\zeta)$ by
154 a parametric dependence $\xi = V_s t, \eta = a \sin(\gamma t + \beta), \zeta = a \cos(\gamma t + \beta)$ where t is
155 the time and β is a phase angle. The velocity components of a point of a helix are
156 given by the temporal derivatives of the coordinates of the point:

$$157 \quad \mathbf{V}_h = V_s \mathbf{i}_\xi + a\gamma \cos(\gamma t + \beta) \mathbf{i}_\eta - a\gamma \sin(\gamma t + \beta) \mathbf{i}_\zeta. \quad (3)$$

158 In view of (3) the term "a larva's velocity" may refer to the two related but
159 different velocities. One of them pertains to the mean velocity of a larva V_s in the
160 preferable direction of motion $O\xi$, termed here "the swimming velocity". The
161 absolute value of the instantaneous velocity of the larva's motion along the helical
162 path V_h and the swimming velocity V_s relate as:

$$163 \quad V_h = \sqrt{V_s^2 + (a\gamma)^2}. \quad (4)$$

164 It should be noted that a larva never moves along a regular helix with a straight
165 axis $o\xi$. However, if the radius of curvature of the mean trajectory of a larva is

166 much larger than the local pitch of the corresponding helix, then equations (3) can
167 still be used as an approximate model of larval helical motion.

168 Two dimensional (2D) trajectories of a larva shown in Fig. 3-4 can be used
169 for approximate estimating of the diameter of a helix $d_h = 2a$ and its temporal
170 period T . Even if the actual direction of the swimming velocity of a larva is
171 unknown, the projection of a cylindrical helix on the plane of a lens is confined by
172 two parallel lines with the distance between them equal to the diameter of the
173 helix (Figures 4-5). The temporary period of the helix can be estimated by
174 calculating the time at which a larva moving along the helix makes a full turn. For
175 example, using data from Figure 4, the radius of the helix a can be estimated as
176 approximately three diameters of a larva; whereas the temporal period of the helix
177 T can be estimated as approximately 1 s.

178 Estimating the swimming velocity V_s from 2D images remains problematic
179 because the mean trajectory of a larva is not in the plane of the lens (see Fig. 5).
180 However, if the maximal velocity V_h , the period of a helix T and the radius of a
181 helix a are known, then in view of (4) the swimming velocity V_s can be
182 calculated as:

$$183 \quad V_s = \sqrt{V_h^2 - (a\gamma)^2}. \quad (5)$$

184 Wendt [28] suggested measuring V_h by filming the motion of larvae in a shallow
185 depth of field and in such way that only a small portion of a larva's trajectory is in
186 focus. In such a case the distance which a larva covers in focus divided by the
187 corresponding time gives an estimate of V_h . According to Wendt [28] for *B.*
188 *neritina* $V_h \approx 5$ mm/s. In such a case the swimming velocity V_s can be estimated
189 as approximately $V_s = 3$ mm/s. Qian et al. [2] estimate the swimming velocity of
190 *B. neritina* as 1 mm/s; whereas we observed values V_s varying from 0.5 to 6
191 mm/s.

192 It should be noted that the helical motion is a rough model of a real
193 trajectory of a larva. Moreover, in many occasions larvae makes an unpredictable
194 sharp turn, which can not be modeled rigorously. However, in a flow, the
195 resulting velocity vector of a larva can be represented approximately as a vector
196 sum of the velocity of the fluid and the velocity of a larva in still water. Because
197 the flow velocity is higher than the swimming velocity of a larva then the larva's
198 trajectory in a flow straighten (see Fig. 6 for more detail explanations). Thus, we
199 assume that unpredictable irregularities of a larva's trajectories in still water do
200 not influence significantly the general kinematical pattern of its motion in flow,
201 the case that we study here.

202

203 Mathematical model of the probability of contact

204

205 The problem of calculating the collision efficiency is related directly to the
206 hydrodynamic problem of larval transport in the velocity field of a collector. In
207 this context, two approaches can be used to calculate particle transport in flow:
208 Eulerian and Lagrangian [32]. In the Eulerian approach, the particles are regarded
209 as a continuous phase, which obeys the same laws as the carrier fluid. It is not
210 trivial to include the hydrodynamic forces acting on a particle in the Eulerian
211 approach.

212 In the Lagrangian approach, particles are treated as a discrete phase, in
213 which each individual element moves in a carrier fluid under the action of

214 hydrodynamic forces. The principal steps of the Lagrangian approach are as
215 follows. First, the velocity field around a collector is computed. Then, a number
216 of particles are ejected into the fluid.

217 The Lagrangian approach is computationally intensive and time consuming.
218 However, it allows one to take into account all relevant hydrodynamic forces and
219 to consider, in detail, the mechanics and hydrodynamics of contact. In the present
220 work, we used the Lagrangian approach.

221 For laminar flows, the velocity field induced by a collector can be
222 calculated using the Navier-Stokes equations. The presence in the flow turbulent
223 pulsations of the imbedded sea turbulence makes it impossible to calculate the
224 collision efficiency of a collector on a purely theoretical basis without invoking,
225 directly or indirectly, experimental data. Because of these difficulties, we tacitly
226 postpone the discussion on the influence of turbulence on the collision efficiency
227 of a collector and first formulate the problem for laminar flow conditions. The
228 effect of turbulence of the collision efficiency is discussed later.

229

230 Equations of motion of a self-propelled particle

231 A collector of larvae is assumed to be a long vertical cylinder of diameter D_c
232 (radius R). The cylinder is located in unbounded sea current whose mean
233 velocity vector \mathbf{U}_∞ is normal to the cylinder's axis. The fluid velocity field in the
234 presence of the cylinder is denoted as \mathbf{U} . It is assumed that a particle is small
235 compared to the typical length scale of the variation of the velocity field induced
236 by the cylinder. We considered cylinders with Reynolds numbers $Re_c = U_\infty D_c / \nu$
237 such that $10^2 < Re_c < 10^4$. In this case the flow at the front portion of the cylinder
238 is laminar albeit, as it was noted above, it can be disturbed by embedded
239 turbulence.

240 We consider a larva whose sinking velocity is much lower than the velocity
241 of the sea current U_∞ . Under such circumstances, the distance, which a larva
242 travels in time unit in a horizontal direction, is much larger than the corresponding
243 distance of its sinking. Therefore, in order to simplify the problem formulation,
244 we assumed that a larva moves in a horizontal plane.

245 The collision efficiency of the collector depends on the contact radius of a
246 larva, Δ . Larger radii of contact result in larger probabilities of contact. In our
247 numerical simulations, we assumed $\Delta = d_p / 2$.

248 The trajectory of a larva was described in the coordinate systems shown in
249 Fig. 7. Following the common practice adopted in the theory of aerosols, to
250 calculate the collision efficiency of a cylinder, the initial longitudinal coordinates
251 of all particles $X_o(0) = X^0$ may be chosen to be equal. It is also implied that at a
252 distance $X^0 \gg D_c$, the disturbances introduced by the cylinder in the flow are
253 small compared to the velocity of the undisturbed flow U_∞ .

254 For passive particles, the initial transverse coordinates Y^0 may be chosen to
255 be random numbers that are uniformly distributed in the segment $(-D_c/2, D_c/2)$;
256 whereas the initial angle $\varphi(0) = \varphi^0$ between the axes ox and OX does not
257 influence its trajectory. For a living larva, the angle φ^0 determines the initial
258 direction of the velocity $\mathbf{V}(0)$ (Fig. 8).

259 It is assumed here that far from the collector, larvae move in a certain
 260 preferable direction within an angle $-\Phi < \varphi^0 < \Phi$ ($0 \leq \Phi \leq \pi$) where the initial
 261 angles φ^0 are random numbers distributed within the interval $(-\Phi, \Phi)$ uniformly.
 262 In such a formulation, the angle of the preferable direction of motion becomes one
 263 of the problem parameters whose bearing on the collision efficiency becomes a
 264 part of the investigation.

265 There are three main mechanisms of the collision of a passive particle with
 266 a collector: inertial impaction, direct interception and Brownian diffusion. The
 267 inertial collision is determined by the inertial parameter representing the product
 268 of the Stokes number

$$269 \quad \text{Stk} = \frac{\rho_p}{\rho_f} \frac{d_p^2 U_\infty}{18\nu D_c} \quad (6)$$

270 and a factor $(1 + \rho_f/2\rho_p)$, where ν is the water kinematic viscosity [33].
 271 Typically, for many small marine larvae (including *B. neritina*), the inertial Stokes
 272 parameter is much less than 1/8, a threshold value below which contact of an
 273 inertial point with a cylinder does not take place [11]. For the problem parameters
 274 which are adopted here the Stokes number is of order of $\sim 10^{-2} - 10^{-3}$.

275 Diffusional deposition results from the random Brownian movement of
 276 water molecules that bombard particles and may bring them to a collector. Given
 277 that the own velocity of *B. neritina* is many orders of magnitude higher than its
 278 velocity, which might be induced by the Brownian motion, the mechanism of
 279 diffusional deposition is neglected in the proposed mathematical model of contact.

280 The trajectory of a particle can be described by a derivative of the radius-
 281 vector \mathbf{r} with respect to time t (see Fig. 7):

$$282 \quad \frac{d\mathbf{r}}{dt} = \mathbf{V}, \quad (7)$$

283 where the particle's velocity vector \mathbf{V} can be calculated by solving its differential
 284 equations of motion.

285 It is assumed that the motion of a particle with respect to the fluid is slow
 286 and that the Reynolds number $\text{Re}_p = |\mathbf{V} - \mathbf{U}|d_p/\nu$ is low. Within the framework
 287 of low Reynolds number hydrodynamics and by neglecting the Basset integral, the
 288 equation of motion of a particle in a simplified form can be written as follows
 289 [33]:

$$290 \quad m_p \frac{d\mathbf{V}}{dt} = 3\pi\mu d_p (\mathbf{U} - \mathbf{V}) + \frac{1}{2}m_f \frac{d}{dt}(\mathbf{U} - \mathbf{V}) + m_f \frac{d\mathbf{U}}{dt} + \mathbf{g}(m_p - m_f) + \mathbf{F}_T. \quad (8)$$

291 Here, m_p is the mass of the particle, m_f is the mass of the fluid in the volume
 292 displaced by a sphere, μ is the water viscosity and \mathbf{g} is the vector of the
 293 acceleration of gravity.

294 The last term in the right hand side of (8) represents the thrust of the
 295 particle. The relationship between the velocity \mathbf{V}_h of a particle with respect to
 296 water and the thrust \mathbf{F}_T can be expressed by:

$$297 \quad \mathbf{F}_T = 3\pi\mu d_p k_p \mathbf{V}_h \quad (9)$$

298 where a correction factor k_p takes into account the non-sphericity of a larva's
 299 body and its cilia. Given that even for an immobilized larva, calculating the drag

300 of its ciliated body may be problematic [31], in order to proceed and to obtain at
 301 least an approximate estimate of the drag of a larva's body, it is plausible to
 302 replace it with an equivalent sphere of diameter d_p . For a smooth sphere the
 303 correction factor can be expressed as a function of the Reynolds number
 304 $Re_h = |V_h - U|d_p/\nu$ as follows: $k_p = (1 + 0.158 Re_h^{0.667})$ ($Re_h < 500$) [33]. For *B.*
 305 *neritina*, Re_h is on the order of one, and the correction factor is of the same order
 306 of magnitude.

307 The thruster of a larva creates not only the force F_T but also a torque
 308 hydrodynamic moment M_p . Due to this moment, a larva rotates in still water with
 309 a certain angular velocity ω_p . For a smooth sphere rotating with low Reynolds
 310 numbers $Re_\omega = |\omega_p|d_p^2/\nu$, this moment can be calculated as $M_p = \pi d_p^3 \mu \omega_p$ [35].

311 The water flow in the area influenced by the collector is subject to shear. A
 312 small particle placed in a viscous shear flow is subject to a hydrodynamic
 313 moment $M_s = \pi d_p^3 \mu \omega_s$, which causes the particle to rotate with an angular
 314 velocity ω_s [34]. The latter is equal to approximately half the vorticity vector
 315 $\text{rot } \mathbf{U} = 2^{-1}(\partial U_x / \partial Y - \partial U_y / \partial X)$, i.e., $\omega_s = 2^{-1} k_\omega \text{rot } \mathbf{U}$, where for a low rotational
 316 Reynolds number Re_ω , the correction factor k_ω mainly depends on the
 317 translational Reynolds number Re_p and for $Re_p \leq 200$ is of the order of one [36].
 318 Under the combined action of the two torque moments, M_p and M_s , a particle
 319 begins to rotate with an angular velocity ω , which in turn is associated with a
 320 hydrodynamic moment of fluid resistance to this rotation $M_f = -\pi d_p^3 \mu \omega$.

321 The equation of the conservation of the angular momentum of a rotating
 322 particle is:

$$323 \quad J \frac{d\omega}{dt} = M_f + M_p + M_s, \quad (10)$$

324 where $J = \pi \rho_p d_p^5 / 60$ is the mass moment of the inertia of a sphere. Substituting
 325 the expression for M_f , M_p and M_s into (10), we obtain the differential equation of
 326 a rotating particle with respect to ω :

$$327 \quad \frac{\rho_p d_p^2}{60\mu} \frac{d\omega}{dt} + \omega = \omega_f + \omega_p. \quad (11)$$

328 The rotation of a particle with angular velocity ω_p due to its helical motion is
 329 considered here as a prescribed one. Once the vector of the swimming velocity
 330 \mathbf{V}_s and the parameters of the helix are known, then, in view of (3), the right hand
 331 side of (8) is defined. In such a case, the influence of the angular velocity ω_p on
 332 the velocity of the particle \mathbf{V} can be neglected in the first approximation.

333 Equations (8) and (11) can be further simplified. Different orders of
 334 magnitude of the constituting terms can be revealed by introducing dimensionless
 335 variables $\mathbf{W}^+ = (\mathbf{V} - \mathbf{U})/U_\infty$, $\mathbf{U}^+ = \mathbf{U}/U_\infty$, $\mathbf{V}_h^+ = \mathbf{V}_h/U_\infty$, $t^+ = U_\infty t/D_c$,
 336 $Fr = U_\infty^2/gD_c$, and $\delta = 1 - \rho_f/\rho_p$, yielding:

337
$$\left(1 + \frac{\rho_f}{2\rho_p}\right) \text{Stk} \frac{d\mathbf{W}^+}{dt^+} + \mathbf{W}^+ = -\delta \text{Stk} \frac{d\mathbf{U}^+}{dt^+} + \frac{\delta \text{Stk} \mathbf{g}}{\text{Fr}^2} + \mathbf{V}_h^+, \quad (12)$$

338
$$\frac{3}{10} \text{Stk} \frac{d\boldsymbol{\omega}}{dt^+} = (\boldsymbol{\omega}_f - \boldsymbol{\omega}), \quad (13)$$

339 In (12)-(13) the Stokes number Stk and the buoyancy parameter δ are small
 340 quantities of the first order of magnitude. By neglecting in (12) their product, i.e.
 341 small terms of the second order of magnitude, we obtain the following equation of
 342 motion of a tiny self-propelled particle:

343
$$\text{Stk} \frac{d\mathbf{W}^+}{dt} + \mathbf{W}^+ = \mathbf{V}_h^+, \quad (14)$$

344 or

345
$$\tau \frac{d\mathbf{V}}{dt} + \mathbf{V} = \mathbf{U} + \mathbf{V}_h, \quad (15)$$

346

347 where $\tau = (1 + \rho_f / 2\rho_p) \rho_p d_p^2 / 18\mu$ is the relaxation time (of the order of 10^{-2} s for
 348 the problem parameters). By neglecting all small terms in (12)-(13) and returning
 349 to dimensional notations, we receive purely kinematic equations of motion:

350
$$\mathbf{V} = \mathbf{U} + \mathbf{V}_h, \quad (16)$$

351 and

352
$$\begin{aligned} \frac{d\mathbf{r}}{dt} &= \mathbf{V}, \\ \frac{d\varphi}{dt} &= \omega_f. \end{aligned} \quad (17)$$

353 Eq. (16)-(17) represent the simplest model of the motion of a self-propelled larva
 354 with negligible inertia. The helical motion of the larva is incorporated into (16)
 355 through the velocity V_h , given by (3). Further, depending on a purpose, we use
 356 equations of motion of an inertial larva or a larva which is massless.

357

358

359 Efficiency of a collector

360 Because the motion is considered in a horizontal plane and $\rho_p / \rho_f \sim 1$ within the
 361 framework of our mathematical model the probability of contact E is a function
 362 of four non-dimensional parameters: $V_S^+ = V_S / U_\infty$, $d_p^+ = d_p / D_c$, Φ and Re_c .
 363 The relative importance of each of them on the probability of contact can be
 364 established by numerical simulations.

365 In [12] the collision efficiency of a cylindrical collector of passive
 366 particles for $0.1 < \text{Re}_c < 50$ was analyzed using CFD package COMSOL. In our
 367 work we analyzed the collision efficiency of a cylindrical collector of passive
 368 particles using CFD package AF13. To analyze the probability of contact of self-
 369 propelled particles with a cylinder for $100 < \text{Re}_c < 500$ we used the theory of the
 370 boundary layer [26].

371 AF13 CFD package enables the calculation of both the velocity field
 372 around a cylinder and the particles' trajectories where the motion of an individual
 373 passive spherical particle is described by a simplified equation (15):

374

$$\tau \frac{d\mathbf{V}}{dt} + \mathbf{V} = \mathbf{U}. \quad (18)$$

375

376

377

378

379

Fig. 9 illustrates the streamlines of the flow and the trajectories of particles in the vicinity of a cylinder which are almost indistinguishable within the thickness of the plotted line. It is an indication that for the problem parameters adopted here the inertia of a particle is negligible, and contact may be considered as a result of the direct interception solely.

380

381

382

383

384

385

386

We did not attempt to present systematic data of the probability of contact for passive particles and all of the various problem parameters. This computational task is far beyond the scope of the present paper. As stated in the “Introduction”, our aim was to evaluate the role of larval self-propulsion on a collector’s collision efficiency. For this purpose, we used the approximate methods of the boundary layer theory instead of the direct solution of the Navier-Stokes equations.

387

388

389

390

391

392

393

394

395

396

397

398

In particular, for calculating the velocity field on the front part of a cylinder, both the Blasius and the Pohlhausen’s method provide accurate results sufficient for intended purposes, except for the nearest vicinity of the flow separation point [26]. Given that most collisions of passive particles occur at the upward portion of a cylinder [11-14], we considered this inaccuracy as minor. Here, we used Pohlhausen’s method because it requires less computation compared to the Blasius method [26]. Outside of the boundary layer, the fluid velocity field around a cylinder is calculated as for an inviscid irrotational flow. Because the results of CFD computations illustrated a negligible effect of the particles’ inertia on their trajectories, in most computations, we used equations (16)-(17) although for justification purposes part of numerical simulations was carried out using (13)-(14).

399

400

401

402

403

404

Examples of the calculated trajectories of larvae are shown in Fig. 10. To estimate the probability of contact of larvae with a collector, it is necessary to calculate a large number of trajectories for N_p particles. The influence of this number of the probability of contact is shown in Fig. 11. The collision efficiency calculated for different angles of the preferable direction of motion $0 \leq \Phi < \pi$ is plotted in Fig. 12.

405

406

407

408

409

410

411

412

413

The above numerical examples give clear evidence that the ratio of a larva’s swimming velocity to the flow velocity V_s/U_∞ strongly influences the collision efficiency of a collector. However, these results were obtained for constant values of the ambient flow velocity and variable swimming velocity, whereas the same ratio V_s/U_∞ can be obtained for constant V_s and variable U_∞ . The question arises of whether, in both cases, the collision efficiency coefficient remains the same at least approximately. Fig. 13 provides a positive answer to this question in the range of the flow velocities $U_\infty = 1-10$ cm/s and a larva’s swimming velocities $V_s = 0.05 - 0.5$ cm/s.

414

415

Collision efficiency of a collector with embedded sea turbulence

416

417

418

419

420

There are very little references in the literature to the collision efficiency of cylinder under turbulent flow conditions. In this section we are attempting to estimate the collision efficiency of a cylinder under turbulent flow conditions by using CFD methods. Most of them that are used to calculate the parameters of the turbulent flow, are based on the Reynolds average Navier-Stokes equations

421 (RANSE) that are combined with equations of the kinetic energy k and the
422 energy dissipation rate ε (e.g., $k-\varepsilon$, $k-\omega$ and Reynolds Stress models).

423 A frequently used model to describe particle motion in a turbulent flow is the
424 eddy interaction model (EIM) developed in [37], which is represented in most of
425 the AF13 codes (see also [38]). According to [37], the integral scale L_ε of the
426 largest eddies feeding the turbulent system far from the collector, the turbulent
427 kinetic energy k and the energy dissipation rate ε are related as $L_\varepsilon = C^{3/4}k^{3/2}/\varepsilon$,
428 where $C = 0.09$ for $k-\varepsilon$ and $k-\omega$ models. Far from the collector, the turbulent
429 intensity I of the embedded sea turbulence and the mean fluid velocity \bar{U}_∞ are
430 related as $k = 1.5(\bar{U}_\infty I)^2$. If the characteristic size of a larva d_p is much less than
431 the Kolmogorov length η_k [39], then the larva sits in a laminar flow, and the
432 hydrodynamic forces acting on it can be calculated as for a laminar flow. The
433 ratio of the largest scale L_ε of the turbulent flow to the smallest scale η_k are
434 related through the Taylor micro-scale Reynolds number Re_λ
435 $L_\varepsilon/\eta_k = (Re_\lambda^2/15)^{3/4}$. Fully turbulent flow requires Re_λ to be larger than
436 approximately 100; the highest Reynolds numbers measured in tidal channels are
437 $Re_\lambda \approx 2000$ [40-42]. Table 2 presents typical values of the turbulence in the sea
438 upper mixing layer [40-42].

439 Once the diameter of a particle is less than the Kolmogorov length and the
440 rest of the parameters of turbulence are also defined, AF13 enables the calculation
441 of the trajectories of a large number of particles that begin their motion in the
442 nodes of the computational grid. In a turbulent stochastic random walk model
443 from one node may start a number of particles. Due to the randomization of the
444 problem, all their tracks are different.

445 We computed the collision efficiency of a cylinder with embedded
446 turbulence for $Re_c = 500$. It is known that even for a laminar flow with
447 $Re_c > 200$ the wake of a long cylinder is unsteady and can not be considered as
448 two dimensional. In a flow with embedded turbulence in its wake are definitely
449 three dimensional. Therefore our 2D calculations can not reproduce faithfully the
450 three dimensional (3D) structures of the wake of the cylinder. However, because
451 we consider collisions of particles with a vertical cylinder, it is expected that three
452 dimensional structures will not affect significantly the collisions on the front part
453 of the cylinder where most of them take place. The computed values of the
454 probability of contact E obtained using $k-\omega$ model of turbulence for realistic
455 parameters of the sea turbulence are given in Table 2.

456

457 Discussion

458

459 The general features of contact of a larva with a protruding collector are
460 explained in further detail in schematic Figures 14 and 15. Motion of a larva in a
461 vortical flow and its deviation from a streamline of a collector due to rotation is
462 illustrated in Fig. 14. Fig. 15 illustrates the typical scales of the contact problem.
463 Far from a collector, the trajectory of a larva is determined by the sea current and
464 the swimming velocity of a larva. In area 1 the hydrodynamic disturbances
465 $U_c = U - U_\infty$, which are induced by a collector at a large distance r from it,
466 decay according to the dipole approximation as $U_c \propto U_\infty (R/r)^2$ [43]. In this area

467 the influence of the fluid viscosity on the hydrodynamics is weak and the velocity
 468 field of the collector can be calculated as for a potential flow. The larva moves
 469 approximately along a corresponding streamline or deviates from it depending on
 470 the initial angle of the larva's swimming velocity and on the ratio of its
 471 swimming velocity to the velocity of flow. In the boundary layer of the cylinder
 472 of a thickness δ ($d_p \ll \delta \ll D_c$) the fluid viscosity is essential. In the boundary
 473 layer the larva translates, rotates due to the flow vorticity, and further deviates
 474 from the fluid stream line.

475 From the results of the presented numerical calculations, it follows
 476 that the collision efficiency of a collector is a growing function of the non-
 477 dimensional parameter V_s/U_∞ . Strictly speaking, this dependence is slightly
 478 nonlinear. However, it can be linearized and represented approximately as:
 479

$$480 \quad E \approx A + B \frac{V_s}{U_\infty}, \quad (19)$$

481 where the coefficients A and B are weakly dependent on the ratio V_s/U_∞ .
 482 Substituting (19) into (2) gives:

$$483 \quad \frac{1}{CS} \frac{dE}{dt} \approx AU_\infty + BV_s. \quad (20)$$

484 The asymptotic formula (20) can be interpreted as follows: for a given unit of the
 485 concentration number, the amount of particles that are collected on a unit area of a
 486 collector is proportional to the velocity of the water flow far away from the
 487 collector and to the swimming velocity of a larva. Both components of (20) are of
 488 the same order of magnitude if $AU_\infty \propto BV_s$ or if $V_s/U_\infty \propto A/B$. Our numerical
 489 simulations demonstrated that for the problem parameters adopted here, $A \ll B$.
 490 Thus, we conclude that even a rather low larval swimming velocity may
 491 drastically influence the larval contact rate with a protruding collector.

492 Collision efficiency of cylindrical collectors of passive particles under
 493 laminar flow conditions for Stokes numbers less than 0.1 and $100 < Re_c < 1700$
 494 vary between $10^{-2} - 10^{-3}$ percents [44]. For a relatively small ratio of the
 495 swimming velocity of a larva to the flow velocity of order of 0.1 the probability of
 496 contact is of order of $\sim 2\%$ (Fig. 13, $E \sim 2\%$ for $V_s/U_\infty = 0.1$). Thus, even
 497 weak swimming increases the probability of contact by 2-3 orders of magnitude.

498 These strong results pertain to laminar flow conditions; whereas real sea
 499 flows tend to be turbulent. Experimental measurements of the collision efficiency
 500 of cylinders under turbulent conditions for Stokes number less than 0.1 are
 501 extremely rare. The available experimental data, which may be relevant to our
 502 problem parameters, shows that for Stokes numbers of the problem less than 0.1
 503 turbulence of intensity $I < 7.5\%$ has no effect on forward collision efficiency of
 504 cylinders [44], [45].

505 Estimates given in Table 2 illustrate that for the realistic problem
 506 parameters turbulence of intensity $I \sim 23\%$ may increase the collision efficiency
 507 of a cylinder also by orders of magnitude compared to the laminar flow
 508 conditions. However, for $V_s/U_\infty \sim 0.1$ the collision efficiency of a collector of
 509 passive particles is about 3 times less than the collision efficiency of the same
 510 collector of self-propelled particles (Fig. 13). Note that for our simulations we
 511 used strong sea turbulence with r.m.s of the velocities of the turbulent fluctuations

512 of the order of 1 cm/s. This velocity is higher than the swimming velocity of the
513 larva under consideration.

514 It should be stressed that the effect of sea turbulence on the collision
515 efficiency of collectors of passive particles and marine larvae is still poorly
516 understood, and more works are needed to clarify this important problem.

517 Our approach is based on observations of the trajectories of slow swimming
518 and almost spherical bryozoan larva *B. neritina*. Thus, a question arises whether
519 in the context of the contact problem this specific larva is a representative
520 example for other species of marine larva. As long as a larva can be viewed as
521 massless self-propelled particle, its motion can be described by kinematic
522 equations similar to (16)-(17). It is not unlikely that they can be applied to other
523 larva, which move with and rotates in a shear flow.

524 We propose a mechanistic and minimalist mathematical model of larval
525 contact with a collector. It takes into account the details of the flow around the
526 collector and the swimming of a larva in a preferable direction of motion. It does
527 not include larval active behaviour as a reaction to light, to various dissolved
528 chemical compounds around the collector, to turbulence as a possible trigger of
529 larval swimming, and other various cues.

530 In this context it should be noted that two alternative approaches to the
531 problem of larval contact with a collector are possible. The first is purely
532 mechanical. Within the framework of this alternative, the rate of contact of larvae
533 with a protruding collector can be calculated theoretically, though inevitably
534 rather approximately. That is the approach that we have taken. However, it can be
535 argued that a larva does not behave as a mechanistic object but simply swims
536 deliberately across the direction of the flow gradient. This second behavioristic
537 alternative, an empirical one, is not the subject of the present paper. However, in
538 the mechanistic model of larval motion, which we have suggested here, at least
539 one important behavioristic aspect is presented: a larva's self-propulsion.

540 We demonstrated that self-propulsion can greatly increase the larva's odds
541 to make contact with a protruding collector, even if the self-propulsion is weak,
542 and the location of the collector for the larva is unknown. From a larva's
543 perspective, to reach a collector and to make contact with it, it is vitally important
544 to be active.

545

546 **Materials and methods**

547

548 **Collection of larvae**

549 Sexually mature colonies of *B. neritina* were collected from floating docks in
550 the Marina of Tel-Aviv, Israel, during the fall and winter period of 2009 and 2010
551 and again during the spring of 2010 following the methodology described in [3],
552 [28]. Colonies were maintained in one liter plastic containers covered with
553 aluminum foil to block light, which induces release of the larvae. Containers were
554 transferred to darkened glass aquaria, where they remained in the dark with no
555 supplemental food at approximately 25°C for a 24-h acclimatization period until
556 the larvae were harvested. Larvae for each experiment were obtained from several
557 colonies to foster genetically heterogeneous populations. Parent colonies used for
558 experiments were maintained in the laboratory and harvested after 3-5 days.
559 Larval release was induced with light. Colonies were removed from the dark,
560 placed in 0.5 liter glass bowls with artificial seawater (approximately 39 ppm,
561 prepared with Red Sea Coral Pro Salt) and then exposed to fluorescent light (two
562 28 W Semi Spiral Day Light lamps, 153 mA each). Larvae appeared within 10

563 min of illumination, and release was complete by 1 h. Because most larvae of
564 *Bugula spp.* are positively phototactic on release, they aggregated at the
565 illuminated side of dishes, a behavior that facilitated collection [28]. Larvae were
566 collected using a glass pipette and placed in approximately 0.2 l before being
567 transferred into the experimental flow tank.

568

569

570 Recording the trajectories of larvae

571 The motion of *B. neritina* larvae was observed in a plane Couette flow
572 apparatus, which consists of a transparent glass aquarium of 1.5x0.2x0.2 m and an
573 electric motor rotating two vertical cylinders. The rotating cylinders move a
574 closed flexible PVC belt. The aquarium is filled with a solution of rectified pure
575 water and sea salt in a prescribed proportion. Larvae were introduced into the
576 experimental tank using a glass pipette. Immediately after release, larvae started to
577 move and did not stop unless they attached to the wall of the tank or to the belt.
578 Larvae trajectories were recorded in still water and in a flow from above and from
579 the side of the tank. Three different types of high-definition digital video cameras
580 were used to film the moving larvae: a Mikrotron 1364 (500 frames/s), Canon 7D
581 (60 frames/s) and Nikon 90 (24 frames/s), all equipped with macro lenses with 60
582 and 100 mm focal lengths. The filmed area was illuminated by disperse low light
583 provided by four identical halogen lamps located approximately 1 m above the
584 free surface of the water. The sensitivity of the cameras' sensors varied between
585 1600-6000 units of ISO equivalent. In most cases, the size of the photographed
586 area was approximately 3x4 cm, and the depth of field varied from a few
587 millimeters to approximately 4 cm.

588

589 Processing of trajectories of larvae in a flume

590 Trajectories of the larvae were digitized using the Image Processing Toolbox
591 of Matlab (<http://physics.georgetown.edu/matlab>). On each frame, the software
592 analyzed the centroid of the object detected by the subtraction method, and the
593 path of a larva was formed as a consequence of centroids using the Matlab track
594 function.

595

596 Mathematical modeling

597 Analytic calculations were performed with pencil and paper. Numerical
598 computations were performed by using commercial CFD package ANSYS-
599 FLUENT 14, C and FORTRAN-77 programming languages.

600 The algorithm of the Polhasen's method [26] was programmed in Fortran 77
601 and executed under Windows using PCs. The differential equations of motion of
602 a larva (15)-(17) were solved numerically using the method of Runge-Kutta of
603 the 4-th order. The adaptive step of integration of the differential equations was at
604 least 10 times less than d_p/V_s , the time which a larva needs to cover a distance
605 equal to its characteristic length. Data fitting was performed in MatLab 7.

606 CFD numerical simulations were performed using a multiprocessor
607 workstation SiliconGraphics CPU Intel Xeon with 16 GB Memory. Calculation of
608 the collision efficiency of a collector of passive particles was carried out using
609 AF13 with a grid with quadrilateral cells. Particles start their motion far from the
610 cylinder, in the nodes of a computational grid with cells clustered to the cylinder.
611 In the numerical examples provided here the maximal number of quadrilateral
612 cells was 6,939,645 with the average element quality larger then 0.70. The
613 average size of a quadrilateral cells adjusted to the cylinder was about

614 $h = d_p / 200$. From each cell 20 particles begin their motion to the cylinder. The
615 criteria of contact of a particle with the cylinder was formulated as
616 $(l - d_p / 2) \leq \Delta + h$, where l is the distance from the center of the particle to the
617 cylinder. The sensitivity of the results to the size of the mesh was justified by
618 comparing the calculated drag coefficient of the cylinder C_D with available
619 experimental measurements.
620

621 **References**

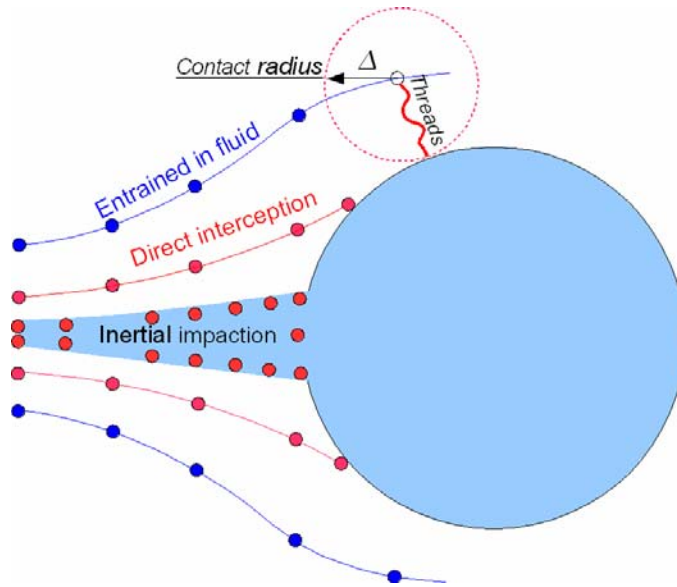
- 622 1. Mullineaux LS, Garland ED (1993) Larval recruitment in response to
623 manipulated field flows. *Mar Biol* 11: 667-668.
- 624 2. Qian PY, Rittschof D, Sreedhar B, Chia F (1999) Macrofouling in
625 unidirectional flow: miniature pipes as experimental models for studying the
626 effects of hydrodynamics on invertebrate larval settlement. *Mar Ecol Prog Ser*
627 191: 301-303.
- 628 3. Qian PY, Rittschof D, Sreedhar B (2000) Macrofouling in unidirectional flow:
629 miniature pipes as experimental models for studying the interaction of flow and
630 surface characteristics on the attachment of barnacle, bryozoan and polychaete
631 larvae. *Mar Ecol Prog Ser* 207: 109-121.
- 632 4. Mullinaux LS and Butman CA (1991) Initial contact, exploration and
633 attachment of barnacle (*Balkans Amphitrite*) cyprids settling in the flow. *Mar Biol*
634 110: 93-103.
- 635 5. Perkol-Finkel S, Zilman G, Sella I, Miloh T, Benayahu Y (2006) Floating and
636 fixed artificial habitats: effects of substratum motion on benthic communities in a
637 coral reef environment. *Mar Ecol Prog Ser* 317: 9-20.
- 638 6. Perkol-Finkel S, Zilman G, Sella I, Miloh T, Benayahu Y (2008) Floating and
639 fixed artificial habitats: Spatial and temporal patterns of benthic communities in a
640 coral reef environment. *Est Coast Shelf Sci* 77: 491-500.
- 641 7. Harvey M, Bourget E, Ingram RG (1995) Experimental evidence of passive
642 accumulation of marine bivalve larvae on filamentous epibenthic structures.
643 *Limnol Oceanogr* 40: 94-104.
- 644 8. Harvey M, Bourget E (1997) Recruitment of marine invertebrates onto
645 arborescent epibenthic structures: active and passive processes acting at different
646 spatial scales. *Mar Ecol Prog Ser* 153: 203-215.
- 647 9. Rittschof D, Sin TM, Teo SLM, Coutinho R (2007) Fouling in natural flows:
648 cylinder and panels as collectors of particles and barnacle larvae. *J Exp Mar Biol*
649 *Ecol* 348: 85-96.
- 650 10. Abelson A, Denny M (1997) Settlement of marine organisms in flow. *Annu*
651 *Rev Ecol Syst* 28: 317-339.
- 652 11. Fuchs NA (1964) The mechanics of aerosols. Pergamon Press, Oxford. 408 p.
- 653 12. Humphries S (2009) Filter feeders and plankton increase particle encounter
654 rates through flow regime control. *PNAS* 106: 7882-7887.
- 655 13. Palmer MR, Nepf HM, Pettersen TJR (2004) Observation of particle capture
656 on a cylindrical collector: implication for particle accumulation and removal on
657 aquatic systems. *Limnol Oceanogr* 49: 76-85.

- 658 14. Haugen NEL, Kragset S (2010) Particle impaction on a cylinder in crossflow
659 as a function of Stokes and Reynolds numbers. *J. Fluid Mechanics* 661: 239-261.
- 660 15. Abelson A, Weihs D, Loya Y (1994) Hydrodynamic impediments to
661 settlement of marine propagules, and adhesive-filament solution. *Limnol*
662 *Oceanogr* 39: 164-169.
- 663 16. Abelson A (1997) Settlement in flow: upstream exploration of substrata by
664 weakly swimming larvae. *Ecology* 78: 160-166.
- 665 17. Hadfield MG, Koehl MA (2007) Rapid behavioral responses of an
666 invertebrate larva to dissolved settlement cue. *Biol Bull* 207, 28-43.
- 667 18. Pasternak Z, Blasius B, Abelson A (2004) Host location by larvae of a
668 parasitic barnacle: larval chemotaxis and plume tracking in flow. *J Plankton Res*
669 26: 487-493.
- 670 19. Qian PY, Lau SC, Dahms HU, Dobretsov S, Harder T (2007) Marine biofilms
671 as mediators of colonization by marine microorganisms: implications for
672 antifouling and aquaculture. *Mar Biotechnol* 9: 399-410.
- 673 20. Yavin Y, Zilman G, Miloh T (1994) A feasibility study of ship
674 maneuverability in the vicinity of an obstacle: stochastic control approach.
675 *Comput Math Appl* 28: 63-76.
- 676 21. Yavin Y, Frangos C, Miloh T, Zilman G. (1997) Collision avoidance by a ship
677 with a moving obstacle: computation of feasible command strategies. *J Optim*
678 *Theory Appl* 93: 59-74.
- 679 22. Jonsson PR, Andre C, Lindegarth M (1991) Swimming behavior of marine
680 bivalve larvae in a flume boundary-layer flow: evidence for near-bottom
681 confinement. *Mar Ecol Prog Ser* 79: 67-76.
- 682 23. Karp-Boss L, Jumars PA (1998) Motion of diatom chains in a steady shear
683 flow. *Limnol Oceanogr* 43: 1767-1773.
- 684 24. Zilman G, Novak J, Benayahu Y (2008) How do larvae attach to a solid in a
685 laminar flow? *Mar Biol* 154: 1-26.
- 686 25. ANSYS-FLUENT 13 Theory and User Guide (2010), Ansys Inc.
- 687 26. Schlichting H (1979) Boundary layer theory. 7th Ed. McGraw Hill Co. 535 p.
- 688 27. Sobol IH (1994) A premier for the Monte Carlo Method. CRC Pres, 430 p.
- 689 28. Wendt DE (2000) Energetics of larval swimming and metamorphosis in four
690 species of *Bugula* (Bryozoa). *Biol Bull* 198: 346-356.
- 691 29. Kosman ET, Pernet B (2009) Diel variation in the size of larva of *Bugula*
692 *neritina* in Field population. *Biol Bull* 216: 85-93.
- 693 30. Koeugh HJ, Black KP (1996) Predicting of scale of marine impact:
694 understanding planktonic link between populations. In: *Detecting Ecological*
695 *Impact*, R. Schmitt and C.W. Osenberg (eds), Academic Press 199-234 pp.
- 696 31. Emlet RB, Strathmann RR (1985) Gravity, drag and feeding current of small
697 zooplanktons. *Science* 228:1016-1017.
- 698 32. Seinfeld JH, Pandis SN (1998) Atmospheric chemistry and physics. John
699 Wiley & Sons, NY, 1326 pp.
- 700 33. Maxey MR and Riley JJ (1983) Equation of motion for a small rigid sphere in
701 a nonuniform flow. *Phys Fluid* 26: 883-88 .

- 702 34. Shiller L, Naumann A. (1933) Uber die grundlegenden berechnungen bei der
703 schwerkraftaufbereitung . Verein Deutscher Ingenieure 77: 318-355.
- 704 35. Happel J, Brenner H (1983) Low Reynolds number hydrodynamics with
705 special application to particulate media. Noordhoff, Leyden. 572 p.
- 706 36. Bagchi P and Balachandar S (2002) Effect of free rotation on the motion of a
707 solid sphere in linear shear flow at moderate Re. Phys Fluid 14: 2719-2737.
- 708 37. Gosman AD, Ioannides E (1983) Aspect of computer simulation of liquid
709 fuelled combustors. Journal of Energy 7: 482-490.
- 710 38. Dehbi A (2008) A CFD model for particle dispersion in turbulent boundary
711 layer flows. Nuclear engineering and design 238: 707-715.
- 712 39. Tennekes H, Lumley JL (1972) A first course in turbulence. MIT Press. 390 p.
- 713 40. Gargett AE (1989) Ocean turbulence. Annu Rev Fluid Mech 21: 419-451.
- 714 41. MacKenzie BR, Leggett WC (1993) Wind based model for estimation the
715 dissipation rates of turbulent energy in aquatic environments: empirical
716 comparisons. Mar Ecol Prog Ser 94: 207-216.
- 717 42. Jiménez J (1997) Oceanic turbulence at millimeter scales. Sci Mar 61 (Supl.
718 1): 47-56.
- 719 43. Lamb H (1945) Hydrodynamics, 6th Ed. New York: Dover. 533 p.
- 720 44. Asset G, Kimball D, Hoff M (1970) Small particle collection efficiency of
721 vertical cylinders in flows of low-intensity turbulence. American Industrial
722 Hygiene Association Journal 31: 331-334.
- 723 45. Stuempfle AK (1973) Impaction efficiency of cylindrical collectors in laminar
724 and turbulent fluid flow. Part III. Experimental. Edgewood arsenal technical
725 report AD909457, Department of the Army, Headquarters, Edgewwod Arsenal,
726 Maryland, 44 p.
- 727
- 728
- 729
- 730
- 731
- 732
- 733
- 734
- 735
- 736
- 737
- 738
- 739

740

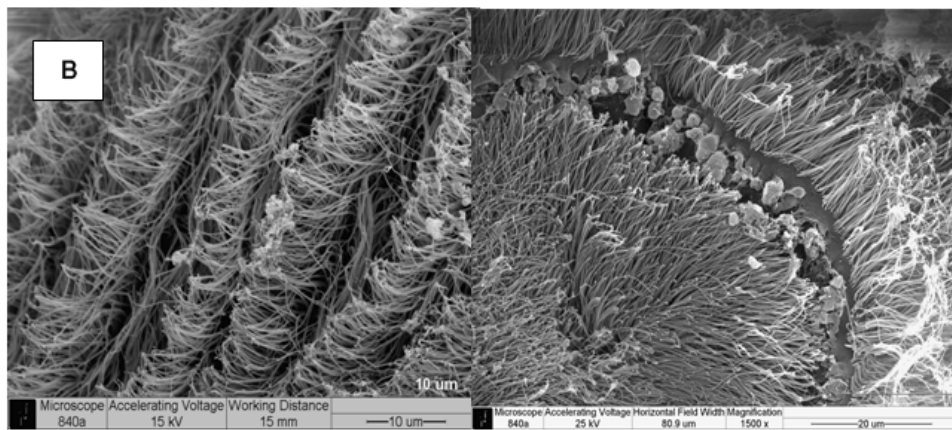
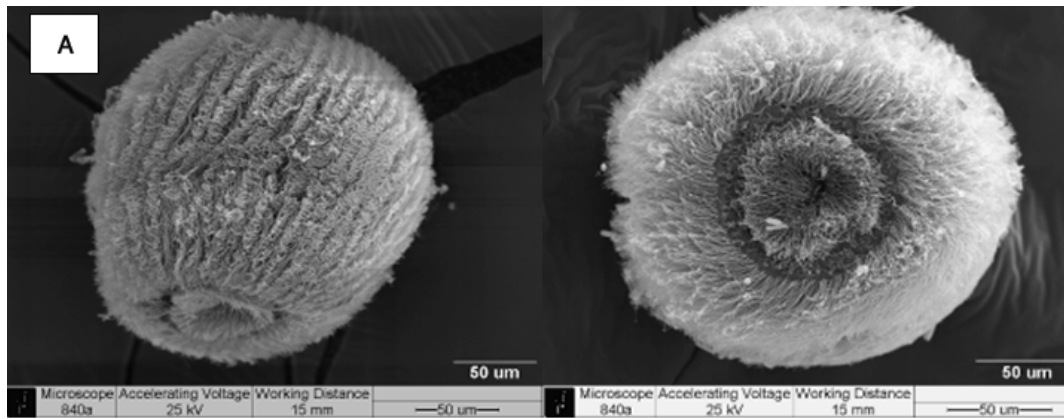
741 **Figures**



742

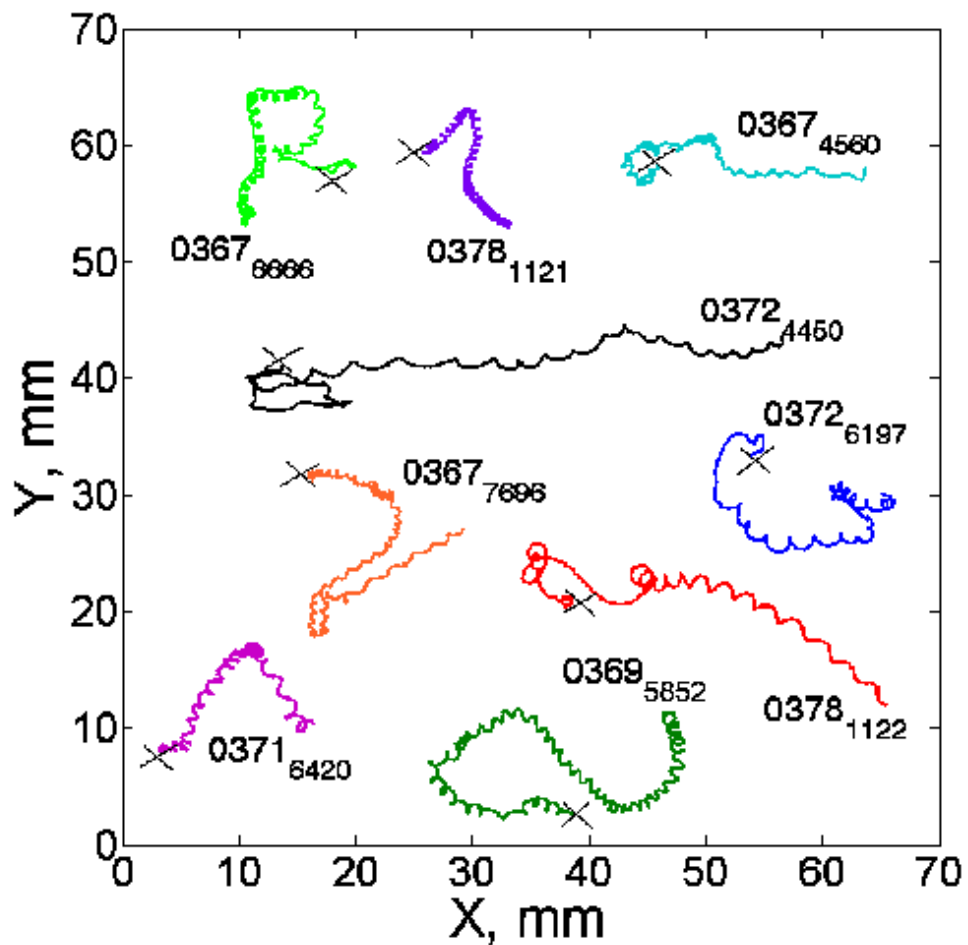
743

744 **Figure 1. Schematic model illustrating the contact of a tiny larva with a large**
745 **collector.** The larva is "entrained" in the flow and follows the fluid streamline. The
746 streamline does not cross the surface of the collector. Contact may take place only if
747 the trajectory of a larva declines from a curvilinear streamline due to the larva's
748 inertia (inertial impaction) or due to its finite size (direct interception). The inertia of
749 a tiny, slow larva is small. For a very low ratio of the characteristic size of the larva
750 to the characteristic size of the collector, the probability of the inertial impaction or
751 direct interception is also very low. Given that not all larvae that contact the
752 collector attach to it and that not all attached larvae survive, the odds of larvae to
753 colonize the collector are seemingly rather low.



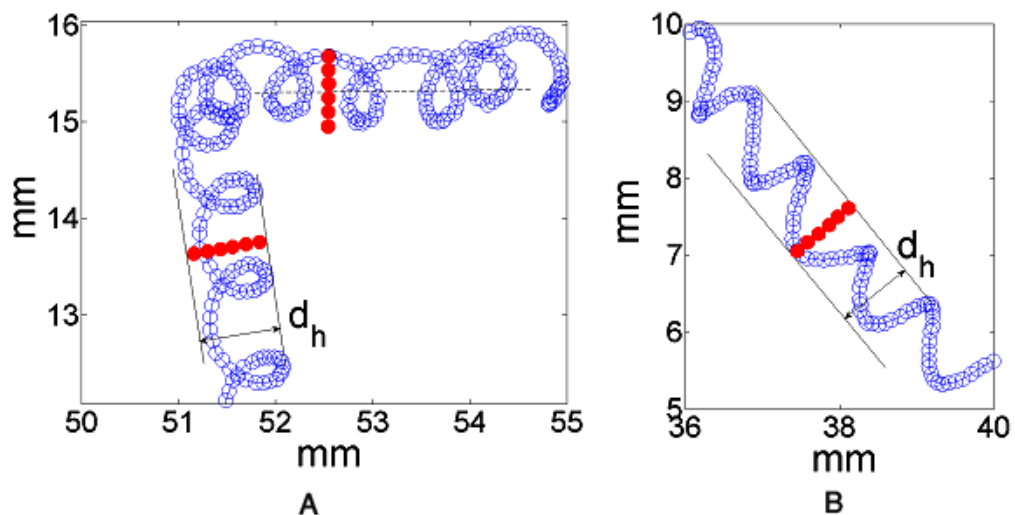
754
755
756
757

Figure 2. Electron microscopy of *B. neritina* larva: A. General view; B. Structure of the ciliated body surface with hair length estimated at 10 μm .



758
759
760
761
762

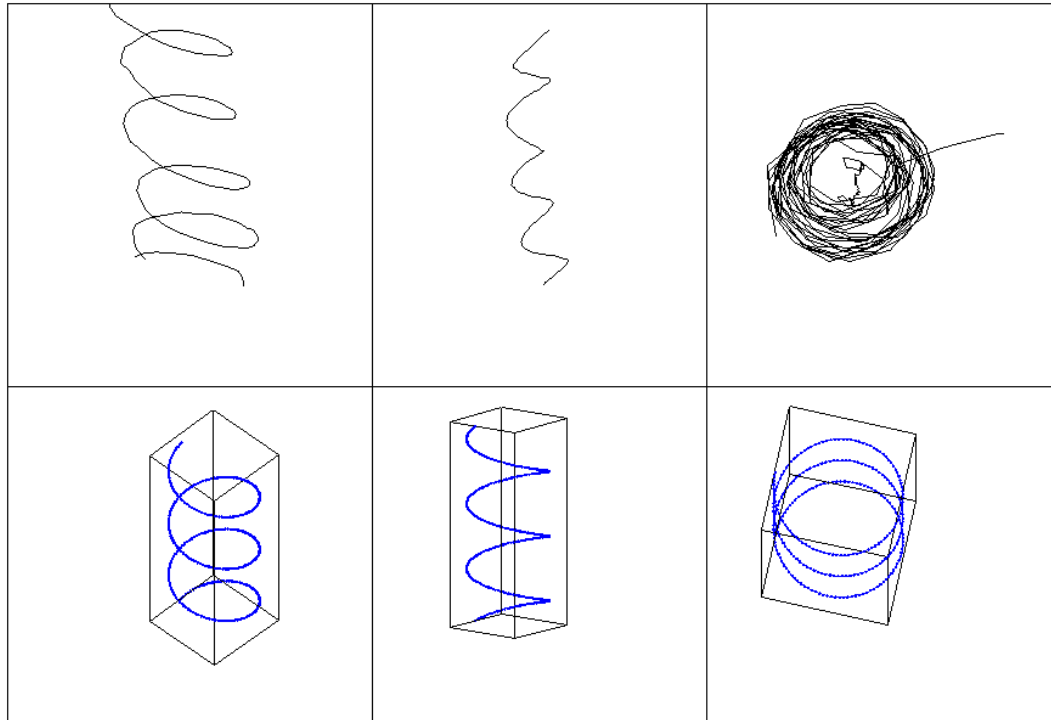
Figure 3. Trajectories of larvae in still water. Because of the additional illumination to one side of the tank larvae move in some preferable direction of motion (from left to right in the figure). × denotes the beginning of the trajectory.



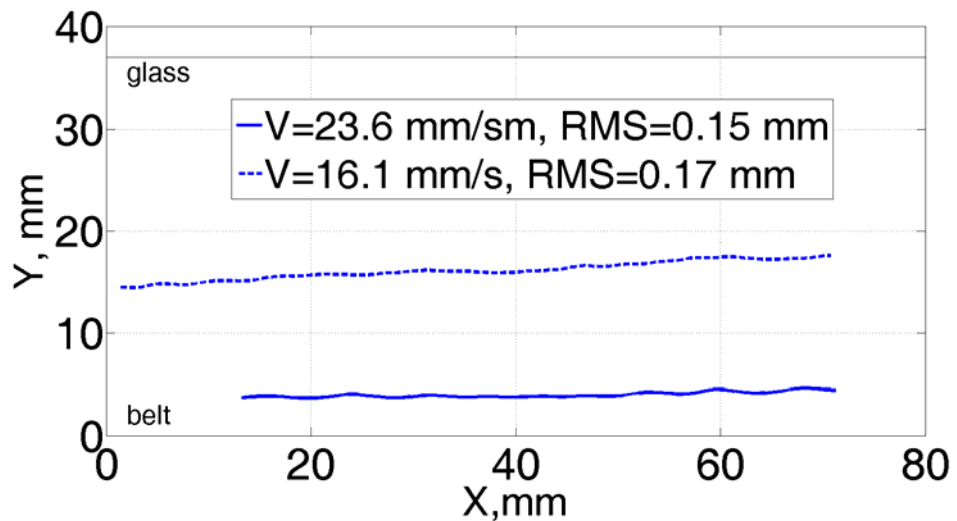
763
764
765
766
767
768

Figure 4. Enlarged parts of trajectories: A. 0367₆₆₆₆; B. 0369₅₈₅₂. Open circles show the consequent position of a larva at a resolution of 1/24 s. Filled circles depict the estimated transverse displacement of larvae in the direction perpendicular to the preferable direction of swimming measured in diameters of a 20

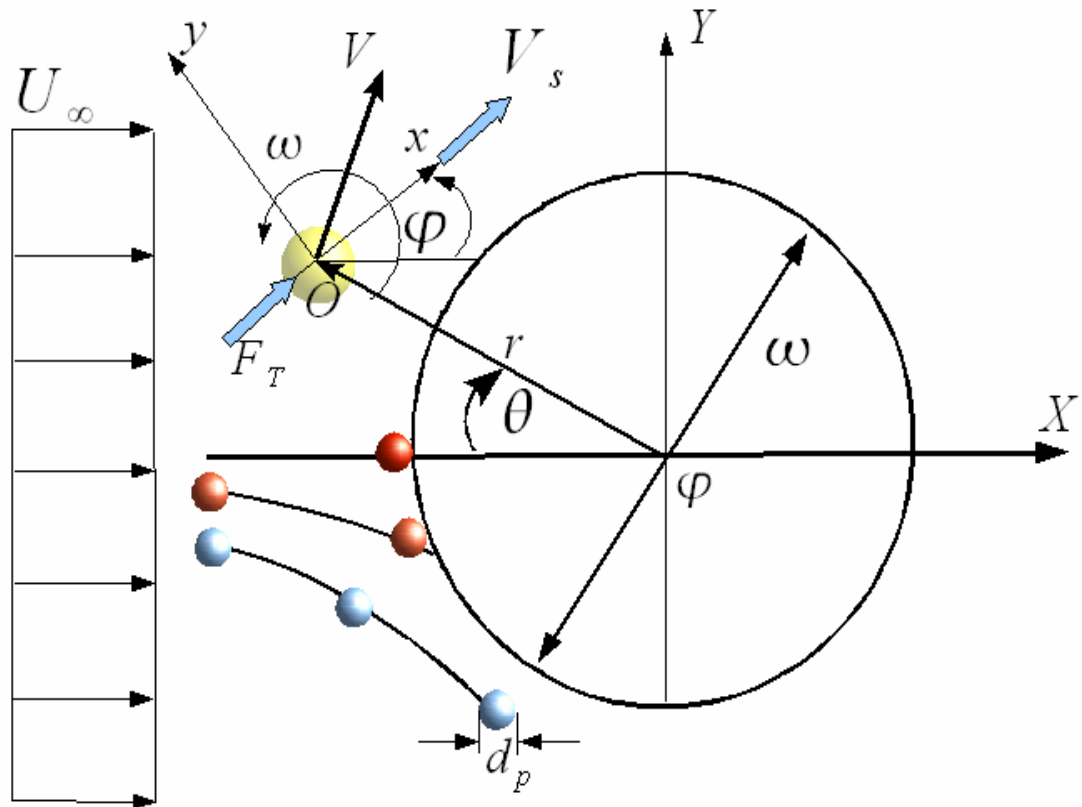
769 larva. The distance $d_h = 2a$ between two parallel lines bounding the trajectories
 770 can be considered as geometric characteristic of the helix.
 771



772
 773
 774 **Figure 5. Patterns of larval motion.** The upper row represents experimental 2D
 775 larval trajectories. In the lower row, the 3D helices are seen from different angles.
 776

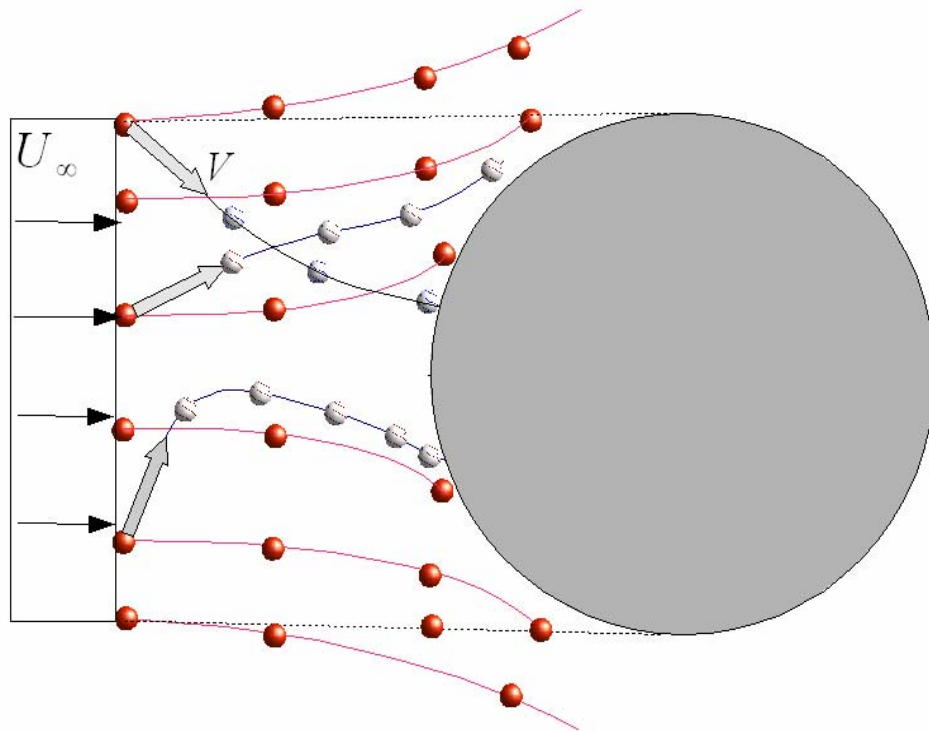


777
 778 **Figure 6. Motion of larvae in Couette flow.** The fluid motion in the Couette
 779 flow apparatus is unidirectional. Therefore, a deviation of a larva's trajectory from
 780 a straight line is due to its own motion. The root mean square of the deviation is of
 781 the same order of magnitude as the deviation of a larva from the axis of a helix
 782 (see Figures 4-5 of larval helical motion).
 783



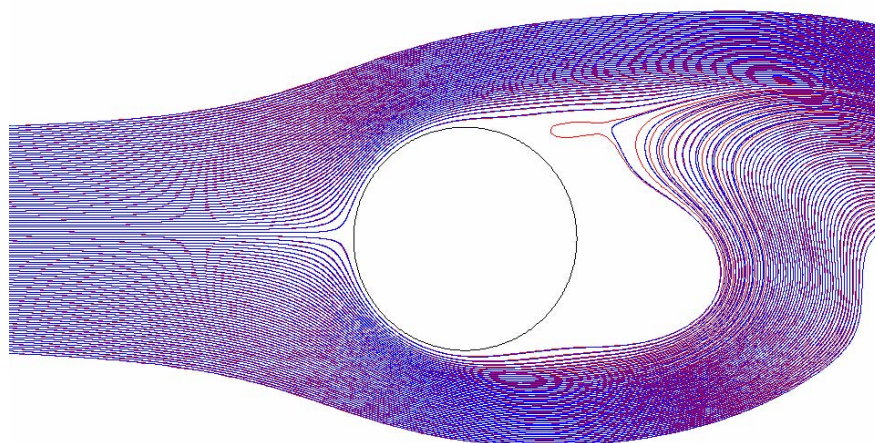
784
785

786 **Figure 7. Orthogonal coordinate systems.** The system OXY is fixed in a
787 collector and the system oxy is fixed in the larva. The initial o of the coordinate
788 system oxy coincides with the center of inertia of the larva and moves with linear
789 velocity V , the larva's velocity. The coordinate of the initial o in the coordinate
790 system OXY is defined by the radius-vector $\mathbf{r}(X_o, Y_o)$. The coordinate system
791 oxy rotates as a whole, with the angular velocity of the larva ω . The angle
792 between the axes ox and Ox is denoted as φ . The angle between the radius vector
793 and the negative direction of the longitudinal axis is denoted as θ . The larva
794 moves with the swimming velocity V_s under the action of a propulsion force F_T .
795



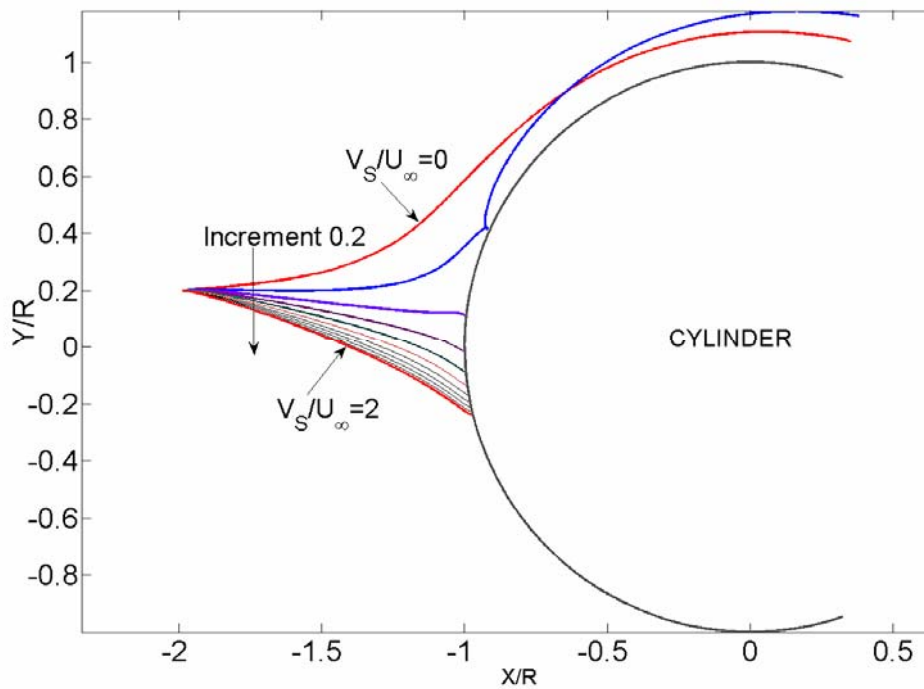
796
797
798
799
800
801
802

Figure 8. Schematic trajectories of passive particles (red spheres) and of living larvae (light spheres). Arrows indicate the initial direction of the vector of self-propulsion.



803
804
805
806
807
808

Figure 9. Streamlines (red) and trajectories of particles (blue) near a cylinder ($Stk = 4.4 \times 10^{-3}$, $Re_c = 200$).

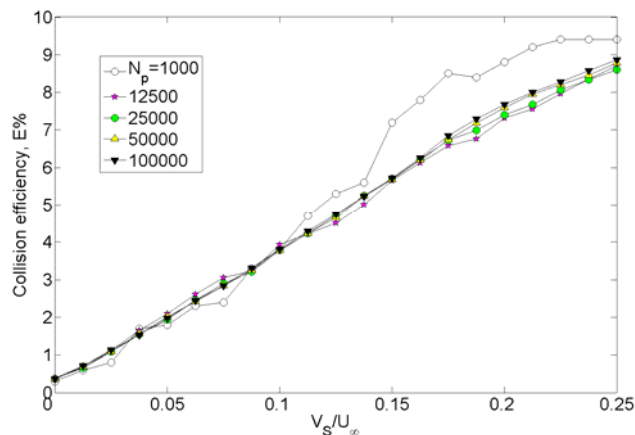


810

811

812 **Figure 10. Trajectories of a self-propelled particle beginning the motion with**
 813 **initial angle of turn $\varphi = -30^\circ$ and initial coordinate $Y/R = 0.2$**
 814 **($Stk = 2.2 \times 10^{-3}$, $Re_c = 100$). The trajectories can cross or touch the collector**
 815 **depending on the ratio of the swimming velocity of a larva to the velocity of the**
 816 **current and the initial angle of turn. Note that for a passive particle all trajectories**
 817 **are identical to that pertaining to the line $V_S/U_\infty = 0$.**

818



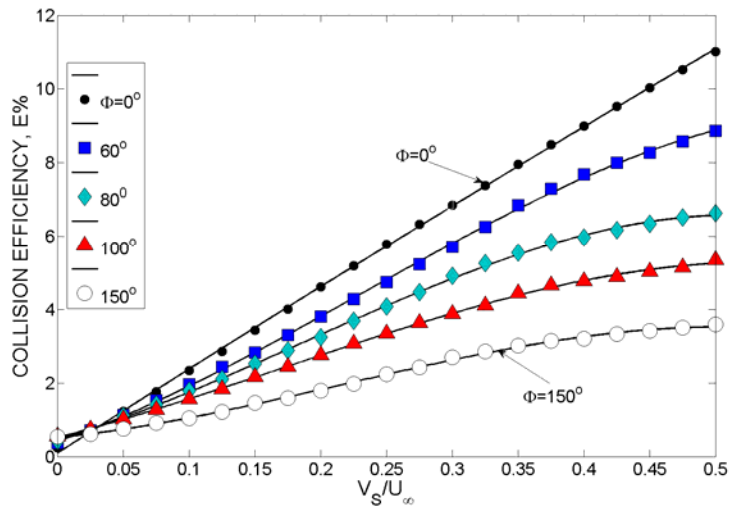
819

820

821 **Figure 11. Collision efficiency as a function of the ratio V_S/U_∞ for a different**
 822 **number of simulated particles N_p ($Stk = 2.2 \times 10^{-3}$, $Re_c = 100$, $\Phi = 45^\circ$). To**
 823 **attain a high accuracy of the collision efficiency coefficient, it is necessary to**
 824 **simulate the trajectories of a large number of particles of the order of**
 825 **$N_p = 10^4 - 10^5$.**

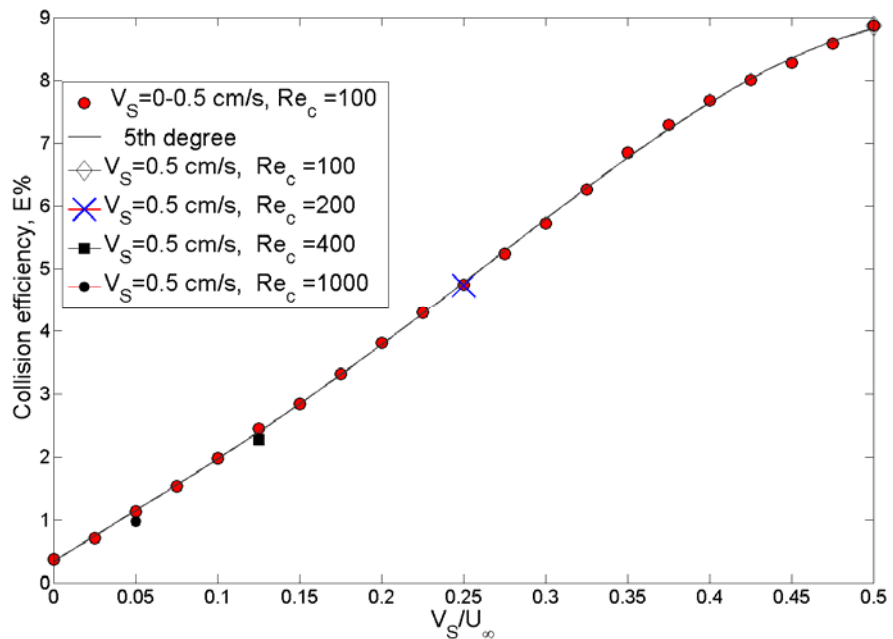
826

827
828
829
830



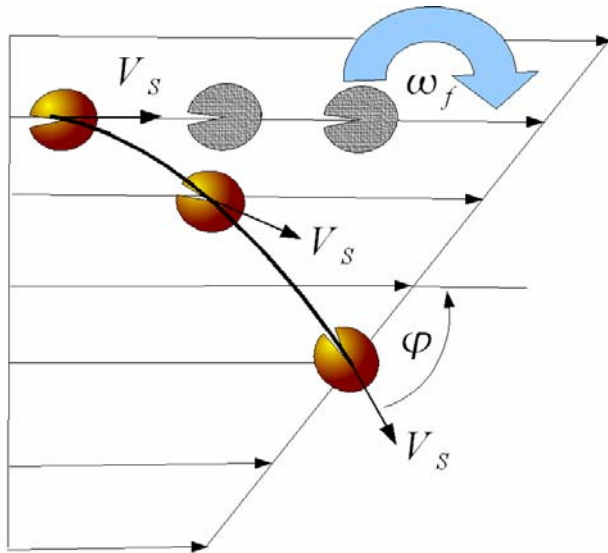
831
832
833
834
835
836
837
838
839
840

Figure 12. Collision efficiency as a function of the ratio V_S/U_∞ for different angles Φ ($Stk = 2.2 \times 10^{-3}$, $Re_c = 100$). The collision efficiency depends on the preferable direction of motion. For angles $0 \leq \Phi \leq 60^\circ$, the influence of the initial preferable direction of motion on the collision efficiency is weak; for angles $60^\circ \leq \Phi \leq 180^\circ$, the influence increases. Further numerical simulations were carried out for $\Phi = 60^\circ$ when the initial angle of larval direction varies randomly as $-60^\circ < \varphi < 60^\circ$.



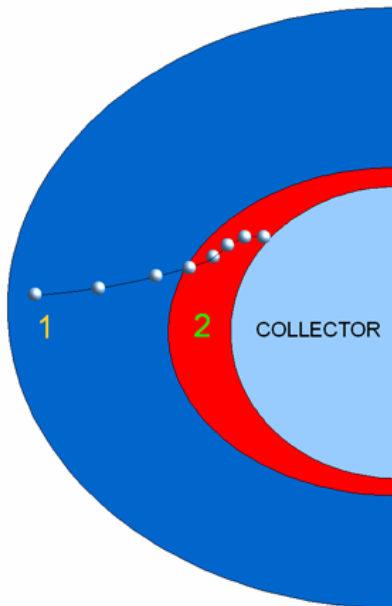
841
842
843

Figure 13. Collision efficiency as a function of the ratio V_S/U_∞ for V_S -const or U_∞ -const ($Stk = 2.2 \times 10^{-3} - 2.2 \times 10^{-2}$).



844
845
846
847
848
849
850
851
852
853
854
855

Figure 14. Motion of small passive and self-propelled particles in viscous shear flow. Locally the flow in the vicinity of the particles can be viewed as unidirectional. In a unidirectional flow a small passive particle translates with the flow and rotates with an angular velocity ω_f . Within the framework of the low Reynolds number hydrodynamics the center of a passive rotating particle moves rectilinearly. For a self-propelled particle the angle φ between the vector of the swimming velocity \mathbf{V}_s and the particles direction of motion varies with time. The sum of the two velocity vectors $\mathbf{U} + \mathbf{V}_s$ forces the particle to move along a curvilinear trajectory instead to continue a rectilinear motion.



856
857
858
859
860
861
862

Figure 15. Fluid domains of influence of a collector on a larva. 1. Area of influence of a collector on a larva where the fluid viscosity can be neglected; 2. The boundary layer of the collector where the fluid viscosity have to be taken into account.

863 **Tables**

864

865 **Table 1. Characteristic range of the parameters for small-scale, wind driven**
 866 **oceanic turbulence**

L_ε	ε	η_k	u_k	T_k	Re_λ
2-100 m	$10^{-4} - 10^{-1} \text{ cm}^2/\text{s}^3$	0.3-2 mm	0.3 – 3 mm/s	5-0.1 s	$200 - 10^4$

867

868 **Table 2. Parameters of sea turbulence and the collision efficiency of a**
 869 **cylinder collecting passive particles calculated using the $k - \omega$ model.**
 870

\bar{U}_∞	D_c	Re_c	d_p	L_ε	η_k	ε	I	Re_λ	E
cm/s	cm	-	μm	m	mm	cm^2/s^3	%	-	-
5	1	500	200	2.2	1.5	2×10^{-3}	23	500	0.67%